Energies of the X- and L-valleys in $In_{0.53}Ga_{0.47}As$ from electronic structure calculations

Gabriel Greene-Diniz, M. V. Fischetti, and J. C. Greer

Citation: Journal of Applied Physics **119**, 055707 (2016); doi: 10.1063/1.4940740
View online: http://dx.doi.org/10.1063/1.4940740
View Table of Contents: http://aip.scitation.org/toc/jap/119/5
Published by the American Institute of Physics

JOURNAL OF APPLIED PHYSICS **119**, 055707 (2016)

Energies of the *X*- and *L*-valleys in $In_{0.53}Ga_{0.47}As$ from electronic structure calculations

Gabriel Greene-Diniz,[1] M. V. Fischetti,[2] and J. C. Greer[1]
[1]*Tyndall National Institute, Lee Maltings, Prospect Row, Cork, Ireland*
[2]*Department of Materials Science and Engineering, University of Texas at Dallas, 800 West Campbell Road RL10, Richardson, Texas 75080, USA*

(Received 11 October 2015; accepted 13 January 2016; published online 5 February 2016)

Several theoretical electronic structure methods are applied to study the relative energies of the minima of the *X*- and *L*-conduction-band satellite valleys of $In_xGa_{1-x}As$ with $x = 0.53$. This III-V semiconductor is a contender as a replacement for silicon in high-performance *n*-type metal-oxide-semiconductor transistors. The energy of the low-lying valleys relative to the conduction-band edge governs the population of channel carriers as the transistor is brought into inversion, hence determining current drive and switching properties at gate voltages above threshold. The calculations indicate that the position of the *L*- and *X*-valley minima are ~1 eV and ~1.2 eV, respectively, higher in energy with respect to the conduction-band minimum at the Γ-point. © *2016 AIP Publishing LLC*. [http://dx.doi.org/10.1063/1.4940740]

I. INTRODUCTION

Transistors fabricated using materials with high charge-carrier mobility have attracted attention over the past several decades. Higher transistor channel-mobility permits a given current drive to be maintained at lower applied voltage, enabling the same performance relative to silicon while reducing power consumption.[1] In recent years, high-κ materials have been introduced as replacements to thin SiO_x layers as gate dielectrics. The high-κ oxides help to alleviate leakage currents arising from gate tunneling by enabling the use of thicker oxides, while maintaining the same gate capacitance. Eliminating the native oxide from the gate-stack gives renewed relevance to the question as to whether performance gains can be achieved with high mobility channel materials without increasing fabrication complexity and costs. Attention is focused on III–V compound semiconductors and germanium as *n*- and *p*-type channel materials, respectively, due to their higher electron and hole mobilities.[1] Of these, $In_{0.53}Ga_{0.47}As$ is considered a promising "post-silicon" material for *n*-typed transistors thanks to its compatibility with existing complementary metal-oxide-semiconductor (CMOS) process technologies and to its improved performance.[2] Much of the performance gain results from the lower electron effective mass in these materials, which leads to a higher electron mobility relative to silicon. However, it should be noted that the carrier mobility becomes a less meaningful figure of merit for sub-10 nm channel lengths, as transport approaches the quasi-ballistic regime and, consequently, scattering becomes less important. For quasi-ballistic transport, the current is dominated by the density of states (DoS) in the source and by the carrier injection velocity. Nonetheless, in both regimes, mobility-limited (diffusive) and quasi-ballistic transport, it is necessary to determine the DoS within an energy window relevant to the transistor operation that includes the conduction band-edge and the low-lying conduction-band "satellite" valleys. This is required in order to describe accurately the formation of the inversion layer in $In_{0.53}Ga_{0.47}As$ metal-oxide-semiconductor field-effect transistor (MOSFET), its capacitance-voltage (CV), and current-voltage (IV) characteristics.

In general, III–V materials have a lower DoS at the conduction band-edge relative to silicon and this is the case for $In_{0.53}Ga_{0.47}As$. The comparatively lower DoS leads to a lower gate capacitance in a MOSFET as the Fermi level moves out of the $In_{0.53}Ga_{0.47}As$ bandgap and into the conduction band-edge at the Γ-valley with application of a gate voltage.[3,4] Along with the lower DoS, a result of a lower effective mass, typically the Γ-valley of III-V semiconductors displays strong non-parabolicity. This is true for the case of $In_{0.53}Ga_{0.47}As$.[5] Efforts made to replace silicon channels with small effective-mass (high electron velocity) materials are hindered by issues related to the "DoS bottleneck."[6] As mentioned above, a small effective mass results in a small DoS, which in turn results in a reduced inversion capacitance. In short-channel (quasi-ballistic limit) $In_{0.53}Ga_{0.47}As$ devices, the larger relative electron velocity is insufficient to compensate for this charge deficiency. This ultimately leads to a significant reduction of the ON-current.[6] At higher gate voltages, the DoS, and hence the capacitance, becomes directly related to the ability to occupy satellite valleys that compensate the lower DoS of the conduction-band edge.

The two lowest lying band-minima of $In_{0.53}Ga_{0.47}As$ above the Γ-valley are at the *X*- and *L*-symmetry points in the Brillouin zone. These valleys have a considerably higher DoS relative to the Γ-valley. As a consequence, a sharp increase in the capacitance occurs as the Fermi level is increased. This results in the occupation of energy states in the valley minima. However, the high field mobility is depressed by the larger occupation of the heavier-mass *L*- and *X*-satellite valleys at higher gate bias.[7] To complicate the analysis, theoretical calculations exhibit a large uncertainty for the calculated values of the energies of the satellite valleys in $In_{0.53}Ga_{0.47}As$. Moreover, it is difficult to extract

this information empirically because of the lack of extensive experimental data.[8] This leads to the use of theoretical predictions for the best estimates for the L- and X-valleys measured from the bottom of the conduction band edge to be $E_L = 0.46\,\text{eV}$ and $E_X = 0.59\,\text{eV}$, as reported for empirical tight binding and k·p calculations, as in Refs. 9 and 10. To predict accurately charge densities, capacitance, and mobility, an accurate knowledge of the energy of the satellite valleys with respect to the conduction band minima is needed.

II. COMPUTATIONAL METHODS

There are limited experimental data available to unambiguously determine the energies of the satellite valleys in $In_{0.53}Ga_{0.47}As$. This is at least partially due to the difficulty in obtaining low defect densities at $In_{0.53}Ga_{0.47}As$/oxide interfaces, thereby complicating the analysis of electrical measurements. To help fill this gap, this paper provides an analysis of the electronic band structure as determined using a variety of computational methods: density functional theory using a local density approximation to the exchange correlation potential (DFT/LDA), hybrid DFT,[11] empirical pseudopotentials, and perturbatively corrected DFT using GW screening (DFT + GW).[12,13] These methods are applied to models of bulk $In_{0.53}Ga_{0.47}As$ including the virtual crystal approximation (VCA) and the use of supercells that accounts for the explicit treatment of the random alloying of indium and gallium atoms on the cation sublattice. In particular, alloying is considered through the use of special quasi-random structures (SQS)[14] and through randomly generated alloy distributions in larger simulation cells. All calculations omit spin-orbit coupling. The effect of spin-orbit interaction on the valence band edges of GaAs and InAs is of the order of several hundred meV, and likewise can be as large as several hundred meV for select conduction bands.[15] However, these effects are not significant at the conduction band minimum and the lowest lying conduction band minima at the L- and X-points.[9] It is assumed that this behavior is retained when alloying and hence spin-orbit effects are not included in our determination of the position of the satellite valleys in $In_{0.53}Ga_{0.47}As$.

Application of the supercell method to the study of disordered alloys can be computationally demanding as a consequence of the very large supercells needed to mimic the random distribution of alloy constituents. To offset this computational complexity, the less demanding VCA is used as a first approximation. A crystal is constructed from a primitive unit cell containing one or more "virtual" (or linearly interpolated) atomic pseudo-potentials. This method has been applied, for example, to the study of electronic structure,[16] thermodynamics,[17] and dielectric properties.[18] The linearly interpolated pseudo-potential is designed to provide an averaged description of the desired alloy stoichiometry. Specifically, the VCA-description of bulk $In_xGa_{1-x}As$ replaces the individual In and Ga pseudopotentials with a virtual "In_xGa_{1-x}" pseudo-potential

$$V_{In_xGa_{1-x}} = xV_{In} + (1-x)V_{Ga}. \quad (1)$$

The use of VCA in this work permits a direct comparison between density functional theory, the empirical pseudo-potential approximation, and GW-corrected DFT. It also permits the investigation of the energies of the local conduction-band minima at the X- and L-symmetry points. The VCA computations also act as a reference for assessing the effect of explicit alloying on the cation sublattice. The two-atom (In_xGa_{1-x}, As) VCA calculations within the DFT/LDA approximation were performed using norm-conserving pseudo-potentials for the Perdew-Zunger approximation to the exchange-correlation (XC) functional. The zinc-blende crystal symmetry and periodic boundary conditions are imposed with the lattice constant fixed to the room temperature experimental value as the VCA approximation is not accurate for the description of bond lengths.[19] The electronic structure for the resulting VCA model of $In_{0.53}Ga_{0.47}As$ is calculated with a kinetic energy cut-off of 60 Ry.

The explicit treatment of random alloying on the cation sublattice requires the use of supercells. This leads to the need to generate random structures that are large enough to produce approximate correlation functions that describe the distribution of nearest neighbors around an arsenic atom bonded to the cation sublattice, and the need to consider more distant atoms corresponding to a random distribution. This requires the use of very large supercells that are not easily amenable to first principle calculations. To avoid this difficulty, Zunger and coworkers proposed crystalline structures or special quasi-random structures that mimic the multisite correlation functions of random alloys.[14] In the following, we use the SQS-2 and SQS-4 16 atom structures to compare DFT + GW and hybrid DFT calculations whereby the In/Ga alloy is explicitly present to some degree. The alloy composition for the SQS-2 and SQS-4 structures is $In_{0.5}Ga_{0.5}As$. The SQS-n structures differ in their atomic configurations which results in different site-to-site correlation functions, with n labeling a specific atomic configuration. Different configurations of atoms in the cell result in different errors for the mth-neighbor correlations compared to a truly random distribution of atom types on the cation sublattice. For example, the SQS-2 structures have larger errors than the SQS-4 for the mth neighbor correlation functions. In addition to the 16 atom SQS-n models, a larger simulation cell is used to investigate the effect of explicitly treating the distribution of indium and gallium sites. This model consists of a 64-atom cell chosen to approximately match the random distribution of nearest neighbor In/Ga atoms about each As atom in the supercell. A $4 \times 4 \times 2k$-point mesh was used for the 16-atom calculations, while a $2 \times 2 \times 2k$-point mesh was used for the 64-atom case. Convergence tests indicate that an equivalent k-point sampling accuracy is achieved in both cases. For all simulations, geometry relaxation (minimization of the energy with respect to the atomic positions) was performed with the lattice parameter held fixed to the room temperature experimental value of 5.87 Å (Ref. 20) to allow direct comparison with the VCA results. The XC functional and plane wave cutoff are also the same as those used for the VCA calculations.

Empirical pseudopotentials express the single-electron Schrödinger equation in Fourier space. The pseudopotential is then described solely by its Fourier coefficients (form factors) that can be empirically determined from known

experimental data.[21] The empirical pseudopotential model (EPM) is applied to the VCA model of $In_{0.53}Ga_{0.47}As$ as EPM methods can correct shortcomings of *ab initio* methods with relatively little empiricism and with excellent computational efficiency. The form factors used in the EPM calculations and details of the method are given in Ref. 22.

To correct for the well-known band gap problem arising when interpreting Kohn-Sham eigenvalues as quasi-particle states in approximate DFT, *GW* methods are also used in our study. *GW* methods[23,24] employ an electronic self-energy Σ to include electron-electron interactions in a quasi-particle Hamiltonian that describes single electron propagation in a many-electron system. The self-energy Σ in this scheme is approximated by an expansion of the dielectric matrix leading to a screened Coulomb interaction. The *GW* approximation enables an accurate treatment of the electronic structure within a quasi-particle description, but it is computationally expensive compared to standard DFT calculations. The DFT + *GW* approach simplifies the *GW* method by assuming the quasi-particle wave functions φ_{qp} are approximated in zeroth order by Kohn-Sham orbitals φ_{KS}. The corresponding Kohn-Sham eigenvalues are then corrected to the first order in the perturbation defined as the difference between the XC potential in the Kohn-Sham equations and the self-energy in the quasi-particle equation[13]

$$\epsilon_{qp} = \epsilon_{KS} + \langle \varphi_{KS} | (\Sigma - V_{xc}) | \varphi_{KS} \rangle. \quad (2)$$

The Kohn-Sham eigenvalues and orbitals obtained from the DFT calculations described previously are used as the starting point for many-body perturbation theory (MBPT) *GW* corrections. The results for convergence tests for the *GW* correction are presented, first focusing on corrections to the VCA model. A set of $2 \times 2 \times 2k$-points in the Brillouin zone are used. A study of the convergence of the quasi-particle optical band-gap with respect to following parameters is performed: the convergence of the screened interaction W, which additionally relies on a sum over occupied and unoccupied states (the calculation of both the dielectric matrix and of the correlation part of the self-energy require a summation over unoccupied states); on the plane-wave energy cut-off; on the size of the dielectric response matrix $\varepsilon_{\mathbf{G},\mathbf{G}'}$; and on the number of points used to perform the fast-Fourier transform (FFT). The plasmon pole approximation (PPA) is used to describe dynamical effects within the *GW* approximation[23] which is used to approximate the inverse dielectric function, as shown in Fig. 1. We have calculated the real and imaginary components of the dielectric matrix using the same DFT parameters already listed and accounting for 46 unoccupied bands (neglecting local fields, i.e., no off-diagonal elements in the dielectric matrix), as shown in Fig. 2. Convergence for the dielectric matrix $\varepsilon_{\mathbf{G},\mathbf{G}'}$ is reached at a dimension of 181×181 reciprocal lattice vectors. Increasing the dimension of $\varepsilon_{\mathbf{G},\mathbf{G}'}$ up to 259×259 results in less than 1 meV change in the band gap energy. Numerical convergence is also obtained with respect to all relevant *GW* parameters. Increasing the number of unoccupied states from 46 to 56 results in less than 1 meV change in the *GW* band gap energy, and a similarly small change in the band gap is

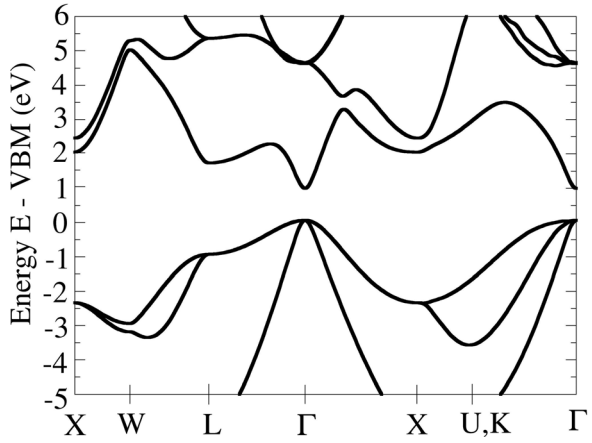

FIG. 1. Real and imaginary parts at the Γ-point component ($\mathbf{G} = \mathbf{G}' = 0$) of the inverse of the dynamic dielectric matrix obtained within the VCA model of bulk $In_{0.53}Ga_{0.47}As$ and plotted as a function of energy.

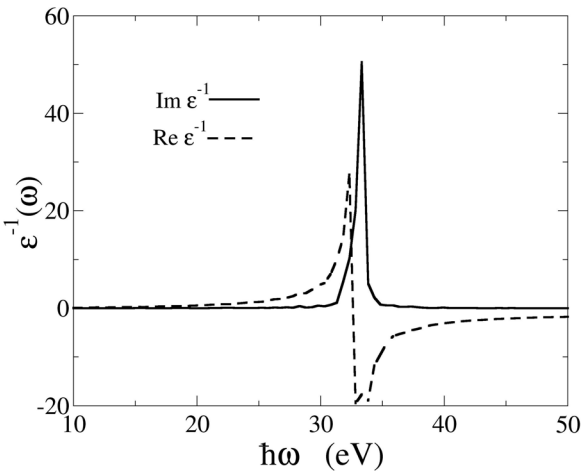

FIG. 2. Band structure calculated from *GW*-corrected Kohn-Sham states using a 2-atom VCA model of $In_{0.53}Ga_{0.47}As$. The *GW*-corrected band gap energy at Γ is 0.92 eV. The valence band maximum is taken as the zero of energy.

observed upon increasing the plane wave cutoff energy to 120 Ry. Following the convergence study, a $12 \times 12 \times 12k$-point mesh is used to determine the quasi-particle band structure. In addition to the VCA cell, the DFT + *GW* calculations are also applied to 16 atom SQS simulation cells. Compared to the two-atom VCA study, a much larger number of unoccupied states (868 in total) is required to achieve adequate convergence for the 16 atom SQS structures. This is attributed to the larger number of occupied states in the 16-atom case, which leads to a much larger number of bands entering the summation required to evaluate the self-energy.[22] As expected, the primary effect of correcting DFT with the *GW* approximation is an upwards shift of the energies of the conduction-band states and a lowering of the energies for valence-band states. DFT + *GW* has been successful in providing better estimates—compared to approximate DFT methods—of the band-gap energies for a variety of group IV, III–V, and II–VI semiconductors.[24–26] It also offers the advantage of being less computationally expensive than the task of iterating φ_{qp} and Σ to self-consistency. This is

the approach chosen as a "benchmark" for the electronic structure methods in this work in cases for which there are no available experimental data.

In addition to the DFT + *GW* calculations on SQS-2 and SQS-4 16 atom supercells, hybrid DFT calculations on these structures were also performed using the Heyd-Scuseria-Ernzerhof (HSE) functional.[11] Hybrid functionals provide an empirical means to "correct the band-gap problem" in Kohn-Sham eigenvalues from approximate DFT by introducing the exact Hartree-Fock exchange into the XC functional. Since the Hartree-Fock method overestimates the energy band gap for well-understood reasons,[27] including a fraction a of the exact exchange into the XC functional allows for a "calibration" of electronic structure calculations against the experimental values of the band gap. A typical value for the exchange mixing parameter is $a = 0.25$. In this work, the mixing parameter is varied between the values of 0.22 and 0.27 and compared to DFT + *GW* and experimental values for the band gap energies.

III. RESULTS AND DISCUSSION

Before studying the satellite valleys in $In_{0.53}Ga_{0.47}As$, we first compare the predicted band gap energies obtained from the various theoretical methods considered. The zero-Kelvin band-gap energy obtained experimentally is $E_g = 0.82$ eV.[5] As anticipated for approximate DFT methods, a significant underestimation of the band gap energy occurs for DFT/LDA in the VCA with $E_g = 0.34$ eV. The empirical pseudopotential method within the VCA provides a much improved estimate of the band gap energy at $E_g = 0.73$ eV and the *GW* correction to the DFT/LDA calculation in the VCA leads to $E_g = 0.92$ eV (Table I). Hence, the empirical pseudopotential and *GW* methods under- and over-estimate the zero Kelvin band gap energy by roughly 100 meV, respectively. The overestimation of the band gap energy with the DFT + *GW* approximation for the low temperature band gap is consistent with previous *GW* studies across a large set of semiconductor materials, with overestimation of the band gaps on the order of a few tens of meV to 100 meV being reported.[26]

Relative to the valence-band maximum, the positions of the conduction band minima do not compare well between the different calculations performed within the VCA. However, in device design applications, the position of the energy minima with respect to the Fermi level for a given gate voltage is the key concern or, similarly, the energies may be expressed relative to the position of the conduction-band minimum when considering an *n*-channel material. In Table I, we list the calculated energetic position of the *L*- and *X*-valleys, relative to the conduction-band minimum at the Γ-point. The three calculations performed with the VCA predict that the energy of the *L*-valley minimum lies 0.72–0.76 eV above the conduction-band minimum. This is reasonably a good agreement with the experimental value, given the variety of approximations used. There is a larger spread in the prediction of the position of the valley at the *X*-point with values ranging between 1.04 and 1.25 eV. For both valleys, the predicted relative energies follow the trend: E(empirical pseudo-potential) > E(DFT/LDA) > E(DFT + *GW*), with all three calculations showing qualitative similarity in predicting that the *L* valley lies below the *X*-valley by 0.32–0.49 eV. The EPM calculations obtained are in agreement with previously published values reported for $In_{0.53}Ga_{0.47}As$ in the VCA.[28,29]

TABLE I. The direct energy gap energy at Γ and the lowest lying conduction band energy minima or "valleys" located at the *L*- and *X*-symmetry points for DFT/LDA, empirical pseudo-potential model (EPM), and DFT + *GW* calculations performed within the VCA. Energies in the first three columns are given relative the valence band maximum at Γ, and energies in the fourth and fifth column are given relative to the conduction band minimum at Γ.

Γ	L	X	ΔL	ΔX	Method
0.34	1.08	1.48	0.74	1.13	DFT/LDA
0.73	1.49	1.98	0.76	1.25	EPM
0.92	1.64	1.96	0.72	1.04	DFT + *GW*

Listed in Table II are the results of the DFT + *GW* and hybrid DFT (DFT HSE) calculations on the 16 atom SQS structures with stoichiometry $In_{0.5}Ga_{0.5}As$ and using the larger 64 atom supercell with a randomly generated composition of $In_{0.53}Ga_{0.47}As$. The calculations are performed using supercells with the consequence that the energy bands are folded in *k*-space. In order to identify the *L*- and *X*-valleys from the SQS and supercell calculations, the energy bands obtained are "unfolded" with the BandUP program using the method described in Ref. 30. In Fig. 3, the 64 atom unfolded DFT/LDA band structure is shown. Once the *L*- and *X*- points of the non-primitive cells are identified from the unfolded band structure, the states at the *k*-points corresponding to these

TABLE II. Tabulation of the conduction band valley energies and their relative energies for explicit alloy models SQS-2 and SQS-4 for 16 atom supercells and an explicit random alloy model for a 64 atom supercell. DFT+*GW* labels perturbatively corrected DFT and DFT HSE includes hybrid exchange with the a parameter specifying the amount of exact exchange mixed into the XC functional.

Γ	L	X	ΔL	ΔX	Method
0.84	1.91	2.04	1.07	1.20	DFT + *GW* SQS-2
0.92	2.03	2.21	1.08	1.29	DFT HSE HSE SQS-2 $a = 0.24$
0.85	1.97	2.16	1.12	1.31	DFT HSE SQS-2 $a = 0.22$
0.87	1.86	2.06	0.99	1.19	DFT + *GW* SQS-4
0.92	1.88	2.18	0.96	1.26	DFT HSE SQS-4 $a = 0.23$
0.88	1.85	2.15	0.97	1.27	DFT HSE SQS-4 $a = 0.22$
0.82	1.83	1.99	1.01	1.15	DFT HSE 64 atom Random alloy $a = 0.24$
0.92	1.91	2.05	0.99	1.13	DFT HSE 64 atom Random alloy $a = 0.27$

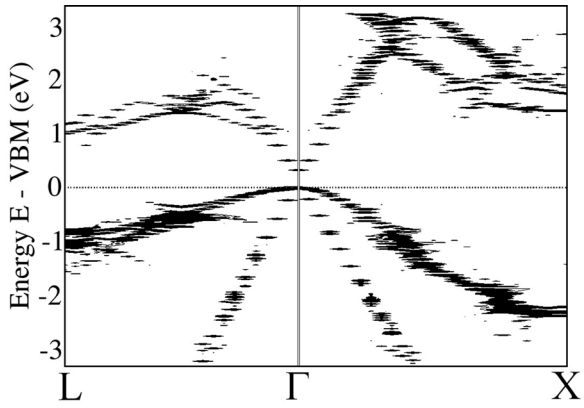

FIG. 3. Unfolded bandstructure of the 64 atom $In_{0.53}Ga_{0.47}As$ supercell calculated using DFT within LDA. Note the distortions along the valence and conduction band edges, particularly at the *L* point. These band splittings are a result of disorder introduced by alloying.

valleys are then selected for the calculations involving the *GW*-correction and the HSE functional, thus yielding accurate estimates for the valleys within the SQS and random alloy models. Compared to the VCA-based calculations, the introduction of explicit alloying on the cation sublattice reduces the DFT + *GW* band gap by 60 meV and 50 meV for the SQS-2 and SQS-4 simulation cells, respectively. This results in a better estimate of the band gap energy compared to the experimental value. The hybrid HSE functional has an empirical element since the mixing parameter may be chosen in order to adjust the calculated band-gap energy. For the SQS-2 structure, we have found that a value of the mixing parameter $a = 0.24$ leads to a band gap equal to that obtained from the DFT + *GW* within the VCA, whereas a value of $a = 0.22$ leads to a band gap similar to the DFT + *GW* calculation on the SQS-2 simulation cell. Similarly for the SQS-4 structure, a value of $a = 0.23$ leads to the same band gap energy as for the DFT + *GW* correction within the VCA, whereas a value of $a = 0.22$ leads to a similar band gap energy as the DFT + *GW* calculation on the SQS-4 simulation cell.

The most notable feature of the explicit alloy models is that they result in a larger energy for the *L*-valley minimum relative to the conduction-band minimum at Γ, when compared against the VCA calculations. The difference E(*L*) − E(Γ) is found to lie within the range of 0.96 eV to 1.12 eV and a significant splitting of the energy levels at the *L*-point is seen from the explicit alloy models. In the explicit alloy models, the splitting of the *L*-point energies is found to be 0.25 eV, whereas the *X*-point splitting is significantly smaller, being less than 10 meV. There is effectively no splitting found for the conduction band minimum at Γ. Clearly, the VCA models cannot capture these explicit alloying effects.

On average, the energy of the *L*-valley relative to the conduction band edge increases to 1.02 eV for the explicit alloy models, greater than the 0.74 eV average value obtained from the VCA calculations. There is a similar but less pronounced increase of the position of the *X*-valley with an energy predicted to lie in the range between 1.13 eV and 1.31 eV, with an average of 1.23 eV. This represents a 90 meV increase over the average VCA-value of 1.14 eV for the *X*-valley. Hence, the explicit alloy models lead to larger energies for both the *X*- and *L*-satellite valleys compared to the VCA calculations. The difference in energy between the *X*- and *L*-satellite valleys is smaller from the explicit alloy calculations than predicted by the VCA. Calculations were also performed with 64 atom cells using hybrid DFT calculations, and similar effects are obtained. The relative energies for the satellite valleys were predicted to lie within a narrow energy range for each alloy model for values from a = 0.22 to 0.27 for mixing exact exchange into the XC functional. However, the position of the *X*-valley reduces as the explicit alloying is included through the use of the supercell models. Overall, the relative positions of the satellite valleys are predicted with a good consistency across the set of theoretical methods applied to the explicit alloy models.

IV. CONCLUSIONS

To summarize, the predicted values of the band-gap energy within the VCA models lie at the higher range of what is expected given the slight overestimation of semiconductor band gaps obtained from DFT + *GW* methods.[26] However, including explicit alloying to the models reduces the error of the DFT + *GW* predictions to within 20 to 50 meV of experimental band gaps. Applying the DFT + *GW* approach to the explicit alloy models results in a significantly larger energy of the *L*-valley relative to the conduction-band minimum as compared to the VCA calculations.[31] For the *X*-valley minima, these effects are qualitatively similar, but are less pronounced.

All theoretical methods we have used predict the *L*-valley minima to be lower in energy than the *X*-valley minima. Combining explicit alloy models with theoretical methods that provide accurate predictions for band-gap energies lead to the conclusion that the *L*-valley minima lie approximately 1 eV above the conduction-band minimum. The *X*-valley minima lie about 200 meV above the *L*-valley minima. This energy difference between the two satellite valleys is approximately one half of what is predicted by the VCA. The DFT + *GW* calculations based on the explicit alloy models estimate the band-gap energies very consistently and in satisfactory agreement with the best known experimental values. This consistency suggests a level of confidence in the calculations of better than 100 meV.

The fact that the energy of the *L*-valley minimum is predicted to lie higher in energy than previously reported bears strong implications on the design of transistors with an $In_{0.53}Ga_{0.47}As$ channel. Lower satellite valley energies imply a larger occupation of the higher-DoS satellite valleys at lower gate voltages. However, if the satellite valleys lie higher in energy, their occupation will become significant only at higher gate voltages. Hence, higher gate voltages are required to exploit the additional current drive associated to the larger electron occupations of the lowest-lying satellite valleys. Understanding and predicting accurately the energy of the satellite valleys—measured from the conduction-band minimum—is required for a correct interpretation of capacitance voltage measurements of high-κ/$In_xGa_{1-x}As$ MOS structures[32] and for designing high-performance transistors.[1]

Note added in proof: Following submission of this manuscript, we became aware of Ref. 33 which applies density functional theory within the framework of the local density approximation and with hybrid functionals to study band bowing in $In_xGa_{1-x}As$ for varying stoichiometry and strain. They find satellite valley energies of $E_L \sim 0.8$ eV and $E_X \sim 1.4$ eV that comparable or slightly larger than our results for $x = 0.53$ and without strain.

ACKNOWLEDGMENTS

This work was performed under the Tyndall Intel Research Collaboration 2013-2015 and additionally supported by the European Union project DEEPEN funded under NMR-2013-1.4-1 Grant Agreement No. 604416. We thank Mr. Conor O'Donnell for demonstrating the use of the BandUP program.

[1]M. Heyns and W. Tsai, MRS Bull. **34**, 485 (2009).
[2]J. A. del Alamo, Nature **479**, 317 (2011).
[3]M. V. Fischetti and S. E. Laux, IEEE Trans. Electron Devices **38**(3), 650 (1991).
[4]Q. Rafhay, R. Clerc, M. Ferrier, G. Pananakakis, and G. Ghibaudo, Solid State Electron. **52**, 540 (2008).
[5]I. Vurgaftman, J. R. Meyer, and L. R. Ram-Mohan, J. Appl. Phys. **89**, 5815 (2001).
[6]M. V. Fischetti, T. P. O'Regan, S. Narayanan, C. Sachs, S. Jin, J. Kim, and Y. Zhang, IEEE Trans. Electron Devices **54**, 2116 (2007).
[7]K. C. Saraswat, C. O. Chui, D. Kim, T. Krishnamohan, and A. Pethe, Int. Electron Devices Meet. **1–2**, 395 (2006).
[8]T. P. O'Regan and P. K. Hurley, Appl. Phys. Lett. **99**, 163502 (2011).
[9]A. Adachi, *Physical Properties of III–V Semiconductor Compounds* (Wiley, New York, 1992).
[10]W. Porod and D. K. Ferry, Phys. Rev. B **27**, 2587(R) (1983).
[11]J. Heyd, G. E. Scuseria, and M. Ernzerhof, J. Chem. Phys. **118**, 8207 (2003).
[12]Paolo Giannozzi *et al.*, J. Phys.: Condens. Matter **21**, 395502 (2009).
[13]A. Marini, C. Hogan, M. Gruning, and D. Varsano, Comput. Phys. Commun. **180**, 1392 (2009).
[14]S.-H. Wei, L. G. Ferreira, J. E. Bernard, and A. Zunger, Phys. Rev. B **42**, 9622 (1990).
[15]M. Cohen and J. R. Chelikowsky, *Electronic Structure and Optical Properties of Semiconductors* (Springer, Heidelberg, 2012), Vol. 75.
[16]T. G. Dargam, R. B. Capaz, and B. Koiller, Phys. Rev. B **56**, 9625 (1997).
[17]S. Degironcoli, P. Giannozzi, and S. Baroni, Phys. Rev. Lett. **66**, 2116 (1991).
[18]L. Bellaiche and D. Vanderbilt, Phys. Rev. B **61**, 7877 (2000).
[19]J. L. Martins and A. Zunger, Phys. Rev. B **30**, 6217 (1984).
[20]O. Madelung, *Semiconductors: Data Handbook* (Springer, Berlin, New York, 2004).
[21]A. J. Williamson, L. W. Wang, and A. Zunger, Phys. Rev. B **62**(12) 12963 (2000).
[22]M. Fischetti, B. Fu, S. Narayanan, and J. Kim, "Semiclassical and quantum electronic transport in nanometer-scale structures: Empirical pseudopotential band structure, Monte Carlo simulations and Pauli master equation," in *Nano-Electronic Devices: Semiclassical and Quantum Transport Modeling*, edited by D. Vasileska and S. M. Goodnick (Springer, New York, 2011), pp. 183–247.
[23]L. Hedin, Phys. Rev. **139**, A796–A823 (1965).
[24]F. Aryasetiawan and O. Gunnarsson, Rep. Prog. Phys. **61**, 237 (1998).
[25]M. S. Hybertsen and S. G. Louie, Phys. Rev. B **34**, 5390 (1986).
[26]M. van Schilfgaarde, T. Kotani, and S. Faleev, Phys. Rev. Lett. **96**, 226402 (2006).
[27]B. T. Pickup and O. Goscinski, Mol. Phys. **26**, 1013 (1973).
[28]M. V. Fischetti, IEEE Trans. Electron Devices **38**, 634 (1991).
[29]K. Kim, P. R. C. Kent, and A. Zunger, Phys. Rev. B **66**, 045208 (2002).
[30]P. V. C. Medeiros, S. S. Tsirkin, S. Stafström, and J. Björk, Phys. Rev. B **91**, 041116 (2015).
[31]G. Greene-Diniz, Ph.D. Dissertation (University College Cork, 2014).
[32]P. K. Hurley, R. D. Long, T. O'Regan, É. O'Connor, S. Monaghan, V. Djara, M. A. Negara, A. O'Mahony, I. M. Povey, A. Blake, R. E. Nagle, D. O'Connell, M. E. Pemble, and K. Cherkaoui, ECS Trans. **33**, 433 (2010).
[33]P. A. Khomyakov, M. Luisier, and A. Schenk, Appl. Phys. Lett. **107**, 062104 (2015).